Nanosecond laser ablation of bulk Al, Bronze, and Cu: ablation rate saturation and laser-induced oxidation

R. Maisterrena-Epstein , S. Camacho-López*
Centro de Investigación Científica y de Educación Superior de Ensenada, Km. 107 Carretera Tijuana-Ensenada, Ensenada, Baja California, 22860, México

L. Escobar-Alarcón
Departamento de Física, Instituto Nacional de Investigaciones Nucleares, Apartado Postal 18-1027, México DF, 11801, México

M. A. Camacho-López
Facultad de Medicina, Universidad Autónoma del Estado de México, Paseo Tollocan s/n esq. Jesús Carranza, Toluca, Estado de México, 50120, México
(Recibido: 20 de marzo de 2007; Aceptado: 21 de julio de 2007)

In this work we report about the characteristics of nanosecond laser ablation, in atmospheric air, of bulk Al, Bronze, and Cu. Average per pulse laser ablation rate and its dependence on ablation depth is presented for these three metals. We will demonstrate and discuss some distinctive features of the ablation saturation effect of the above metals. We will also present results on laser-induced oxidation of the metals which results off the ablation event. We studied the laser-induced oxidation effect through energy-dispersive X-ray spectroscopy (EDS or EDX). The EDS results presented here show that the laser irradiated metals oxidize during the ablation process; the metals oxidize to different degrees showing a strong dependence on the net delivered laser fluence.

Keywords: Metals, Pulsed laser ablation, Laser micromachining, Laser-induced oxidation.

1. Introduction

The laser processing of different kinds of materials is one of the more active research fields around the world. Laser processing of materials offers interesting advantages of fabrication and material transformation over conventional techniques, especially in the materials micro-processing area [1-3]. A wide selection of materials that can be laser-processed includes from dielectrics [4] to metals [5], ceramics [6] to polymers, [7] semiconductors [8], and biological tissue [9]. Some laser-induced material transformations include: refractive index change in transparent materials [10]; oxidation and phase transitions in metals [11]; drilling and surface shaping in metals and ceramics [12]; photo-chemical reactions in polymers [13]; and tissue ablation [14].

Laser ablation can be used to drill tiny holes and channels in metallic plates, which makes this laser technique attractive for fabricating micro-structures for technological applications. However, it is difficult to drill holes with a large aspect ratio. It has been observed that the ablation rate in metals decreases significantly as a function of hole depth, and also it has been noted that oxidation plays a key limiting role during the ablation of deep holes [15].

One of the most commonly observed laser-induced effects in metals is its oxidation. Laser-induced local oxidation has been well studied in metal films for technological applications; an illustrative example of such studies is reported for Chromium films grown on stainless steel using Nd:YAG laser irradiation [16], where the authors show, experimentally, the growth of a Cr_2O_3 film on the stainless steel surface after laser irradiation. Gently laser-induced oxidation, phase-changes and sub-micron structuring of tungsten films has also been demonstrated using Nd:YAG short pulses [17]. These structural transformations generally involve modifications in compositional, optical and electrical properties.

Some technological applications require the fabrication of challenging and demanding micro-structured patterns fabricated in metals and other materials [1-3]. Laser-processing techniques have proved to be quite successful for this task. In this paper we aim to show some relevant characteristics of the laser ablation process of industrial commonly used metal plates of Aluminium, Copper, and Bronze. We will present experimental results on laser ablation rates for these metals and its dependence on channel depth, showing how this dependence leads to an ablation saturation effect; results on laser-induced oxidation for the above metal plates will also be presented. We will show and discuss the dependence of both the ablation and the oxidation effects on the laser irradiation parameters.

2. Experimental

Figure 1 shows the experimental set-up that we utilized to carry out the laser irradiation of the metal samples. We

* corresponding author: camachol@cicese.mx

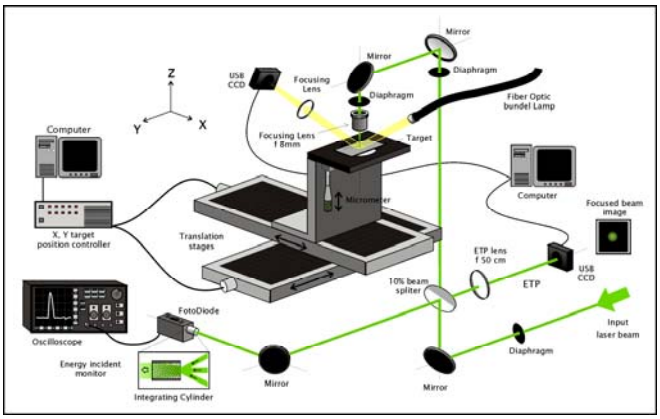

Figure 1. Experimental set up. The main components of the computer controlled laser micromachining station are: laser source, micromachining (focusing) lens, x-y-z stage, energy monitor (photodiode) and CCD for ETP.

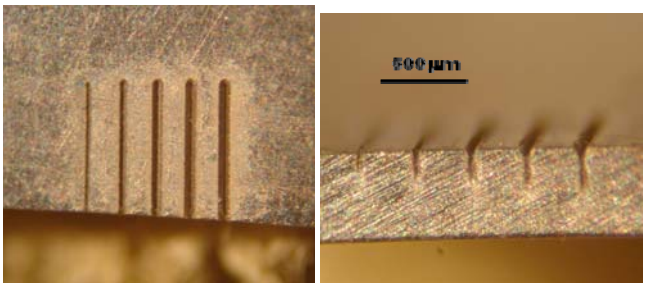

Figure 2. Top (left) and side (right) views of laser ablated straight channels in an Al plate. Each channel is ablated to a different depth using a fix value of both the per pulse laser fluence and the scan speed (i. e. we use a constant net fluence). Deeper channels are ablated by scanning the sample multiple times along the same location while displacing the sample upwards (the laser beam is incident from above) after completion of every round trip scan.

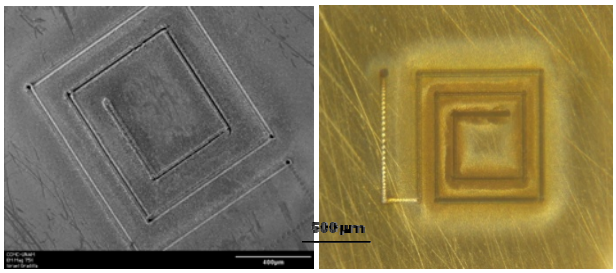

Figure 3. Swirl patterns recorded on bronze at a fixed per pulse fluence (F_p) of ~ 30 times the ablation threshold fluence (F_p^{th} = 10.3 J/cm^2) [18]. The net fluence at each segment of the swirl is given by the scan speed, the size of the laser beam waist and the pulse delivery rate.

used hand-polished commercially available 0.5 mm thick metal plates of Al, Bronze, and Cu as targets. Energy-dispersive X-ray spectroscopy (EDS or EDX) analysis of a non-irradiated zone on the metal plates provided us with the initial surface chemical composition of the metal targets, for all three materials. The laser source in our experimental set up is a Continuum (Minilite II) frequency doubled (532nm) Nd:YAG laser, with pulses of ~ 9 ns (FWHM) time duration and a repetition rate of 10 Hz. We used an 8 mm focal length (NA=0.5) aspheric lens to focus the beam on target. The laser beam had a diameter of 5 mm (FWHM) at the lens location. The beam waist (6.5 µm measured where the intensity falls to e^{-2} of the axial value) of the focused laser beam was experimentally determined using a 2-D CCD array in combination with an equivalent target plane image system (ETP) as described by Maisterrena-Epstein in [18]. The ETP is a technique that uses the back-reflected portion of the laser beam, together with the microprocessing and the ETP lenses in figure 1, to image the target plane onto a 2-D CCD array. The on target focused beam is both imaged and magnified; the magnification factor is given by the 50 cm focal length to the 8 mm focal length ratio of the pair of lenses. Once captured the laser beam waist image can be digitally processed to accurately measure its shape and size.

The laser processing of the metal plates is carried out in the micromachining station shown above in the schematic of the experimental set-up. The metal samples are conveniently mounted on an x-y-z stage. The x-y stages are both computer controlled (step motor) linear stages (Newport UT100-150-0.1 µm). The z stage is a micrometer linear stage with a 5 µm resolution and it is manually driven. A calibrated (DET210 Thorlabs) photodiode is used to monitor the per pulse energy delivered on target, and a CCD is used to monitor (through the ETP) the plate surface during the whole experiment.

The laser exposure of the metal plates was performed by scanning the samples with the laser beam in the form of either a pattern of straight segments (Figure 2) or a pattern of swirls (Figure 3). In both cases, for a given per pulse laser fluence, any given spot on the sample would be irradiated at a well defined net (or integrated) fluence, which will be determined by the scanning speed. For the case of the swirl pattern, we set a fix per pulse laser fluence and choose a varying speed, which increased from segment to segment; this allowed us to have a single per pulse fluence for the whole swirl, while having ten different net fluences on a single experimental run.

For the straight segments pattern, the scan speed was set to 10 µm/s during the whole exposure, and the fluence per pulse delivered to target was varied from segment to segment if it was required so. For the swirl patterns, the fluence per pulse was set to a fix value for a single swirl until completion, but it was varied from swirl to swirl if required; the scan speed for a given swirl was varied in steps of 2 µm/s from segment to segment. The swirl pattern starts to form at the inner segment, at a scan speed of 2 µm/s, and it completes at the outer segment at a scan speed of 20 µm/s. Given the scan speed, the size of the beam waist and the pulse delivery rate, a total number of pulses between 30 and 3 were delivered at a given spot within the swirl segments.

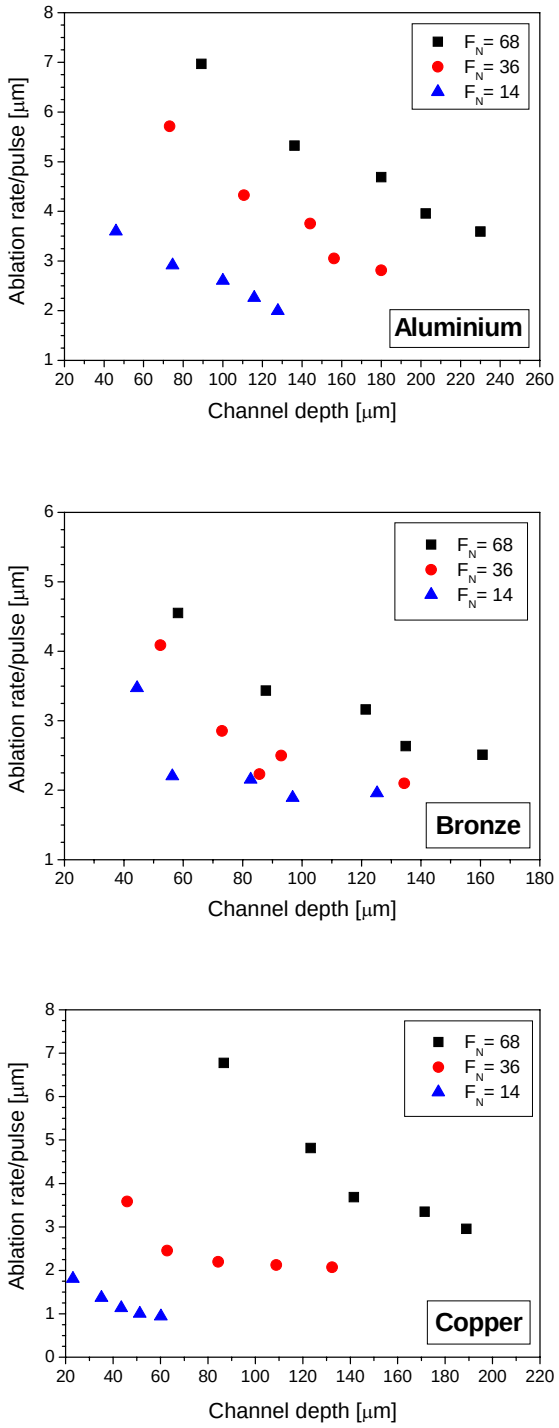

Figure 4. Per pulse (average) ablation rate in Al, Bronze, and Cu as a function of ablation channel depth, for three per pulse fluences normalized to the per pulse ablation threshold fluence of each material (Al: F_p^{th} = 10.4 J/cm^2; Bronze: F_p^{th} = 10.3 J/cm^2; Cu: F_p^{th} = 11 J/cm^2) as reported in [18].

3. Results and discussion

3.1. Ablation rate of Al, Bronze, and Cu

Ablation rate experiments to study the ablation of deep channels were carried out in all three of the above metals. We designed the experiments such that we could form straight line pattern of ablation channels at the very edge of a plate as it is shown in Figure 2a. A series of five channels were ablated running multiple straight line (round trip) scans at a fresh site each time. For every single fresh site we ran first a surface scan followed by a number of deeper scans, where the laser beam waist was re-positioned, for each round trip scan, deeper into the plate by a distance of 20 μm, it is two and a half times the Rayleigh range distance Z_R = 8 μm. The deepest position of the beam waist into the plate with respect to its surface was at ~ 10 Z_R.

Figure 4 shows a plot of the (average) per pulse ablation rate as a function of the ablation depth, for three different fluences per pulse (normalized to the per pulse threshold fluence for ablation of the corresponding material). It can be clearly seen from these results for the three metals how the ablation rate consistently decreases as a function of the ablation depth. There are several features to be noticed, for instance, the ablation rate in all cases drops ~ 50% at the deepest location in the channels, in comparison to the ablation rate obtained close to the surface, for any given delivered fluence. It is also worth to notice that in the case of aluminium, the ablation rate *vs* depth follows the same linear decaying slope for the three delivered laser fluences, which is not at all the case for bronze and copper. In the last two cases, we can see how at the lower laser fluences (F_N = 14, 36) the ablation rate *vs* depth quickly drops and tends to an asymptotic decay, *i. e.* it tends to an almost constant ablation rate in the range between 60-140 m depth. Although at the highest laser fluence (F_N = 68), in these cases of bronze and copper, the ablation rate *vs* depth behavior shows a linear decaying slope too. A material related effect is the following: let's look at a particular depth, say 80 μm (the lowest position of the laser beam waist within the channel).

We can see how for the three metals the amount of material removed per pulse, as a function of the delivered laser fluence, is very distinctive for each material. In the case of aluminium almost doubling the delivered laser fluence, from F_N = 36 to 68, gives only 75% increase on ablation rate capability; as compared to the increase in ablation rate capability given by the two and a half times laser fluence increase, from F_N = 14 to 36. The same analysis show us how in the case of bronze, the increase in laser fluence from F_N = 36 to 68 almost doubles the ablation rate capability, as compared to that of the laser fluence increase from F_N = 14 to 36. The copper case is even more dramatic, since the ablation rate capability for the laser fluence increase from F_N = 36 to 68 gives more than triple, as compared to that of the laser fluence increase from F_N = 14 to 36. Finally, notice that the effect of

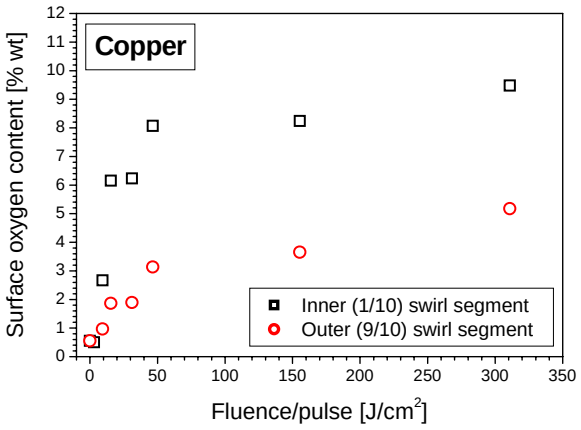

Figure 5. Laser-induced oxidation in copper. EDS measurements of oxygen content were carried out in the close proximity of the ablated swirl segments. The oxygen measurements correspond to two different segments in the swirl: the inner one (the largest net fluence) and the ninth segment out of ten (significantly lower net fluence). It is very important to notice that the per pulse fluence is constant along the whole swirl.

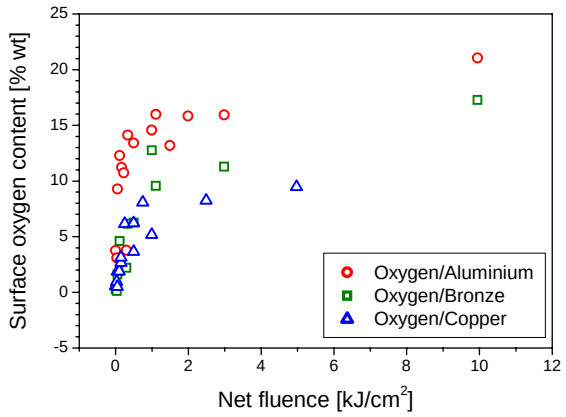

Figure 6. Laser-induced oxidation in Al, Bronze and Cu as a function of net laser fluence. EDS measurements of oxygen content were carried out in the close proximity of the ablated swirl segments.

saturation of the ablation rate starts at the 60-80 μm depth mark for F_N = 14 and 36 in bronze and copper; giving ablation rate saturation values between 1 and 2 μm/pulse. It is clearly not the case for aluminium, where the drop in ablation rate always follows a linear slope, *i. e.* it never saturates in the range of ablation depth achieved in our experiments. It is also worth to point out that for the same set of delivered fluences used in all three metals the deepest channels are ablated in aluminium, so for F_N = 68, we made a 230 μm deep channel in aluminium, a 160 μm deep channel in bronze, and a 190 μm deep channel in copper.

3.2. EDS of the ablated metals

An unavoidable consequence of laser irradiation of metals in the presence of atmospheric air is the effect of laser-induced oxidation. Such an effect takes place as a result of the high temperatures experienced by the metal directly exposed to the laser irradiation; heat dissipation to the surroundings quickly turns in, making it possible to propagate heat to the vicinity, therefore oxidizing a metal area beyond the directly exposed and ablated channel. Figures 5 and 6 show energy dispersive X-ray spectroscopy (EDS) measurements, taken in the close proximity (within 20 μm) to the ablated segments in swirls (see Figure 3) made in aluminium, bronze, and copper. These measurements reveal the chemical composition changes that occur on the metal surface as a function of the net delivered fluence. It can be clearly seen how the general trend is a rapid increase of the oxygen content at the lower laser fluences, followed by an asymptotic increase for higher fluences. Figure 5 shows a quite interesting effect, although the laser fluence per pulse is the same throughout the whole swirl, when sampling the first and ninth segments, the degree of oxidation is larger at the first segment, which goes in well agreement with the fact that the net fluence is larger in the first than in the ninth segment due to the slowest scan speed at that very segment as compared to outer ones.

Figure 6 shows the degree of oxidation as a function of net laser fluence for the three metals aluminium, bronze and copper. Notice that for the three cases the rapid increase of oxygen content occurs at net fluences of less than 2 kJ/cm^2; while for larger net fluences the oxygen content still increases but just asymptotically, *i. e.* the oxidation process reaches a saturation regime. The oxygen content for the copper sample changed from a very small initial amount of less than 1% (wt) to a value of up to 10% (wt) at a net fluence of ~ 5 kJ/cm^2. In bronze, the initial oxygen content is also below 1% (wt), however it reaches up to 12% (wt) at a net fluence of 5 kJ/cm^2, and up to 17% (wt) at 10 kJ/cm^2. For the case of aluminium, the initial oxygen content is below 1% (wt) too, but it reaches 16% (wt) at 5 kJ/cm^2, and 21% (wt) for a laser net fluence of 10 kJ/cm^2. It is worth to note that the saturation effect on the oxygen content is probably due to the lack of atmospheric oxygen in the vicinity of the ablation location when high enough fluences are delivered.

From the plots in figure 6, we can also note that the three metals oxidize at different rates with respect the delivered net laser fluence. Notice how aluminium shows the fastest slope in the plot, while bronze and copper oxidize (slower slope) at a more moderate rate as the delivered laser fluence increases. It is also interesting to see that aluminium reaches its oxidation saturation at a higher value (16%) as compared to that of bronze which is lower (12%) and even lower (10%) for copper.

4. Conclusions

The results presented in this work show a series of effects that are present when laser ablation of bulk metals is carried out in atmospheric air. We demonstrated that the average ablation rate per pulse of aluminum, bronze, and

copper decreases as much as 50% for deep ablated channels, in comparison to the ablation rate close to the surface. This fact is a limiting feature on the ability of a laser tool to fabricate high aspect ratio channels. We also demonstrated that the fluence dependent laser-induced oxidation process in the above metals can be well characterized by using EDS measurements. We demonstrated how the oxidation process is fully dependent on the net delivered laser fluence. In all three metal cases there is a well defined rapid increase of the oxygen content, for moderate net laser fluences. This rapid increase is followed by an asymptotic growth of oxygen content for larger net delivered fluences. There is also a consistent saturation of the laser-induced oxidation process, which occurs at net laser fluence ~ 2 kJ/cm^2; such a saturation effect could be due to laser-induced lack of atmospheric oxygen. At fast and high enough delivered fluence; it is possible to consume the available atmospheric oxygen faster than it can diffuse in from the surroundings to the ablation location.

It has been demonstrated throughout this paper that nanosecond pulsed laser ablation of bulk metals, in atmospheric air, involves several effects which are worth to be well studied, especially in the scope of industrial and technological applications.

Acknowledgments

The authors acknowledge support to this work from CONACyT (Grant 51839). We are grateful to Ing. Israel Gradilla for his help with the SEM images.

References

[1] M. C. Gower, Opt. Express **7**, 56 (2000).
[2] H. J. Booth, Thin Solid Films **453-454**, 450 (2004).
[3] N. Rizvi, D. Milne, P. Rumsby, and M. Gower, in: Laser Applications in Microelectronic and Optoelectronic Manufacturing V, **Vol. 3933**, Eds. H. Helvajian, K. Sugioka, M. C. Gower, and J. J. Dubowski. (Proceedings of SPIE, San Jose, 2000) p. 261.
[4] D. Ashkenasi, H. Varel, A. Rosenfeld, F. Noack, and E. E. B. Campbell, Nucl. Instr. and Meth. in Phys. Res. B **122**, 359 (1997).
[5] C. Momma, B. N. Chichkov, S. Nolte, F. von Alvensleben, A. Tunnermann, H. Welling, and B. Wellegehausen, Opt. Commun. **129**, 134 (1996).
[6] H. W. Bergmann, K. Schutte, E. Schubert, and A. Emmel, Appl. Surf. Sci. **86**, 259 (1995).
[7] S. Preuss and M. Stuke, Appl. Surf. Sci. **69**, 253 (1993).
[8] D. von der Linde and K. Sokolowski-Tinten, Appli. Surf. Sci. **154-155**, 1 (2000).
[9] M. D. Feit, A. M. Rubenchik, B.-M. Kim, L. B. da Silva, M. D. Perry, Appl. Surf. Sci. **127-129**, 869 (1998).
[10] J. Qiu, K. Miura, H. Inouye, J. Nishii, and K. Hirao, Nucl. Instr. and Meth. in Phys. Res. B **141**, 699 (1998).
[11] J. L. Jiménez-Pérez, P. H. Sakanaka, M. A. Algatti, J. G. Mendoza-Alvarez, A. Cruz-Orea, Appl. Surf. Sci. **175-176**, 703 (2001).
[12] T. V. Kononenko, S. V. Garnov, S. M. Klimentov, V. I. Konov, E. N. Loubnin, F. Dausinger, A. Raiber, and C. Taut, Appl. Surf. Sci. **109-110**, 48 (1997).
[13] T. Lippert, J. T. Dickinson, S. C. Langford, H. Furutani, H. Fukumura, H. Masuhara, T. Kunz, and A. Wokaun, Appl. Surf. Sci. **127-129**, 117 (1998).
[14] J. Kruger, W. Kautek, and H. Newesely, Appl. Phys. A **69** [suppl.], S403 (1999).
[15] E. Wynne and B. C. Stuart, Appl. Phys. A **76** 373 (2003).
[16] J. Yang, J. Lian, H. Bai, W. Cui, and Z. Guo, ISIJ International **45**, 730 (2005).
[17] R. Evans, S. Camacho Lopez, M. A. Camacho Lopez, C. Sanchez Perez, and A. Esparza Garcia, J of Phys. CS **59**, 436 (2007).
[18] R. Maisterrena Epstein. Caracterización de la ablación láser en metales y PMMA con pulsos cortos (ns) y ultracortos (fs). Tesis de Maestría. (CICESE 2006).